Mediterranean Journal of Basic and Applied Sciences (MJBAS)
Volume 9, Issue 4, Pages 179-206, October-December 2025

Remote Sensing and GIS Support to the natural Hazard Assessment in the Kharga Valley, Central-Egypt

Barbara Theilen-Willige[1]* & Edward A. Dubowski[2]

[1]23683 Scharbeutz, Schleswig-Holstein, Germany. [2]Mansfield, Notts, United Kingdom.
Corresponding Author Email: Barbara.Theilen-Willige@t-online.de*

DOI: https://doi.org/10.46382/mjbas.2025.9414

Article Received: 19 October 2025 Article Accepted: 26 December 2025 Article Published: 28 December 2025

ABSTRACT

Natural hazards occurring in the Kharga valley and its borders in Central Egypt are affecting the maintenance and safety of settlements, infrastructure, and the economic and agricultural development in this arid area An overview of the different geohazards in the Kharga valley is presented including the role and potential of remote sensing and GIS tools for the inventory and monitoring of these hazards such as active dunes and sandstorms, rare flash floods, geodynamic activities (earthquakes), and mass movements. Roads, railroads and fields are prone to sediment covers, mostly because of aeolian activities and fluvial sediment transport in case of rare precipitations. Maps of areas prone to natural hazards are an essential tool for managing their consequences and cascading effects to prevent and prepare exposed populations and infrastructure. Comparative evaluations of data provided by different satellite systems (Landsat, Sentinel 1 and 2, ALOS PALSAR radar images) were carried out from the Kharga valley to demonstrate their value for the assessment of areas prone to geohazards. It can be stated that joint evaluations of satellite images support the monitoring of critical areas.: Landsat RGB images combining thermal bands have shown their value for the detection of wadi beds exposed to flash floods in case of heavy rains, as well as the MNDWI water index image products derived from Landsat and Sentinel 2 data. Using the Hillshading Edge Enhancement Technique (HEET) wadi beds covered by aeolian sediments can be visualized very clearly. From radar data structural and fault information can be gained that are not often visible on optical satellite images because of the sedimentary covers. Combined with earthquake data, structural evaluations support the detection of active fault zones with varying local site conditions in case of stronger ground motion. High resolution satellite images support the location of opening cracks and fissures along the escarpments leading to further block movements and block gliding. Thus, remote sensing data embedded in GIS environment form an important layer in a natural hazard information system providing information that can support natural hazard preparedness, damage mitigation and resilience of the affected communities.

Keywords: Kharga Valley; Central-Egypt; Remote Sensing; Digital Image Processing; GIS; Natural Hazard Assessment; Aeolian Activities, Flash Floods; Mass Movements; Earthquakes; Data Mining, Hazard Preparedness.

1. Introduction

Natural hazards such as, aeolian accumulations, erosion and slope instabilities pose ongoing risks to infrastructure and agriculture in the Kharga valley in Central-Egypt. The Kharga valley is a large, elongated topographic depression oriented in N-S direction. It is situated in the southern Western Desert of Egypt between 24°20.00 N and 26°00`N and 30°20`E and 31°00`E (Figure 1). The topographic depression of the Kharga valley is bordered to the north by the escarpment of Abu Tartur and the plateau of Sinn El Kaddab in the east [1].

A significant agricultural development has taken place in this area comprising various industries that are of great importance to the local economy. In the 1960s, an extended agricultural project was implemented in the area of the El-Kharga Oasis depending on artesian water of the Nubian Sandstone Aquifer System (NSAS) comprising the main groundwater source. As the primary groundwater-consuming sector in New Valley since the 1990s, agriculture was expanded through the exploitation of water resources from the NSAS in response to the expected future population growth.

However, the use of numerous groundwater wells was leading to over-pumping [2]. The cultivated area in New Valley increased due to land reclamation and irrigation management [3]. El-Kharga Oasis comprises about 11,400 hectares under irrigation, with the irrigation system drawing its groundwater from over 1100 shallow wells [2].

Natural hazard assessment requires a systematic collection of data and information (data mining) and integration into a geographic information systems (GIS) data base, whereby the dynamics in the nature of hazards and cascading effects should be taken into account. So far, such a systematic approach has not been documented in publicly available references for the Kharga valley area, only single aspects have been addressed. For example high ground water extraction rates, particularly in this arid region, is leading to land subsidence. The amount of subsidence in the Kharga valley is not yet documented in detail. Along with natural geological processes, anthropogenic activities causing this subsidence, are considered as a geologic hazard [4] [5].

Active dune fields and recent aeolian sand sheet depositions in this hot desert climate form a threat for infrastructure and agriculture. These eolian activities can be observed clearly using remotes sensing data.

Fluvial sediment transport in case of rare precipitations can cause problems for the maintenance of streets and railroads in areas with higher discharge. The affected areas have to be documented to minimize future damages.

Geodynamic activity (including mostly shallow earthquakes and earthquake related secondary effects such as compaction and aseismic movements) can be a reason for small horizontal and vertical displacements. Fault zones with fault related structures such as pull-apart depressions and push-up ridges are crossing the investigation area, often buried under sedimentary covers. These fault zones have the potential to lead to unstable ground conditions. It cannot be excluded that even smaller rifting processes have occurred in the valley subsurface such as observed along the eastern border of the valley within the Sinn el Kaddab plateau.

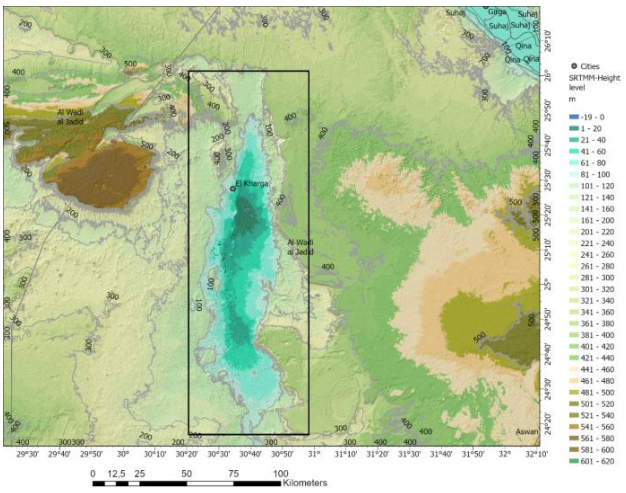

Figure 1. Position of the study area and height level map (based on SRTM DEM data.

The following natural hazards have to be documented and monitored systematically in the Kharga valley (Figure 2):

- Aeolian activity: development of active dune fields, sand sheets, sandstorms, wind erosion forming small, parallel narrow valleys,
- flash floods: flooding in case of rare, locally concentrated precipitations with high intensities,
- mass movements: slope failure along steep scarps (block gliding, development of cracks along the cliffs, gravitational sediment flow, large block displacements) and sediment transport,

Mediterranean Journal of Basic and Applied Sciences (MJBAS)
Volume 9, Issue 4, Pages 179-206, October-December 2025

- aseismic, long-term movements along active fault zones,
- seismic activity: earthquakes causing secondary effects such as compaction or quicksand conditions,
- karst phenomena within limestone outcrops: sinkholes and caves, karst hydrology at the valley borders.

Remote sensing data and tools can support these tasks of documenting and monitoring to a great deal (Figure 2).

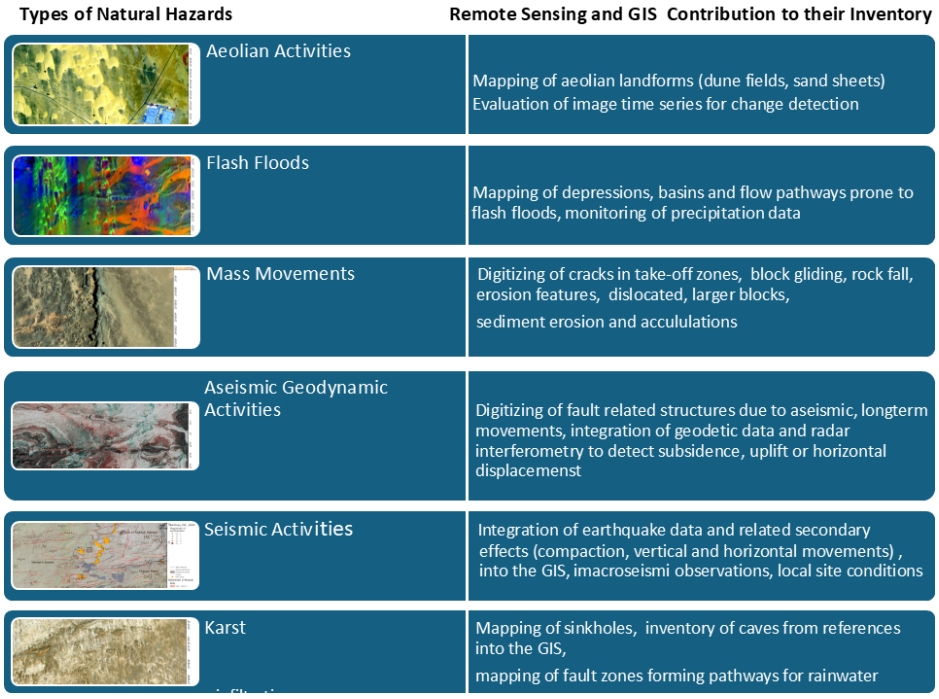

Figure 2. Overview of natural hazards with potential effect on the safety of settlements and infrastructure and the support by remote sensing and GIS tools.

1.1. Study Objectives

Continuous monitoring and systematic spatial and timely documentations of these different natural hazards is essential for land use and hazard mitigation planning.

- Aim of the hazard assessment in the Kharga valley is to identify the various types of hazards and their spatial occurrence. With regard to the future development of this area, the awareness and systematic inventory of natural hazards and their occurrence is important, to support the maintenance of the infrastructure and damage mitigation. Goal of this study, therefore, is to contribute to this inventory using different remote sensing and GIS tools as demonstrated in Figure 2.

- Based on freely available satellite data, partly free software such as SNAP / ESA and QGIS, geodata and references, the long-term monitoring of some of the different natural hazards becomes possible with relatively low costs for a GIS trained staff. This is an important issue, especially for the monitoring of active dunes. For example, by comparing Landsat data available over 5 decades changes in the landscape can be traced.

- Maps of areas prone to natural hazards are an essential tool for managing their consequences and cascading effects and for rising the awareness of exposed populations and infrastructure. Assuming that areas susceptible to

specific natural hazards in the past such as flash floods, will be affected in the future as well, the assessment of exposed sites is necessary. Thus, the goal of this study is to demonstrate how satellite data integrated into a GIS can contribute to the detection of areas prone to hazards such as to the monitoring of aeolian activities, the mapping of flash flood prone areas, and of sites exposed to slope failure as far as possible.

- Research gaps and recommendations for additional data collection are pointed out providing hints for future research activities and systematic GIS integrated data base creations.

- Further on, the different procedures of digital image processing of optical and radar satellite data are crucial for their evaluation content. One goal was directed to testing which kind of processing provides the best results. Of course, the specific digital image processing has to be adapted to the hazard to be monitored and to the arid area conditions in the investigation area. For example, long-wave radar data are better suited for structural-geologic evaluations as they reveal more subsurface information because of the radar signal penetration capabilities than optical satellite data, whereas high resolution, digital enhanced, optical satellite images provide better information about aeolian landforms and activities and slope failure.

1.2. Geographic and Geologic Overview

The Kharga valley and depression with height levels between 20 - 120 m is bordered to the north and east by distinct escarpments reaching height levels over 500 to 600 m. The widespread Quaternary sediments display different formations such as aeolian sand sheets and dunes of different sizes and ages, and fluvial sediments accumulated after rare, heavy rains in this arid environment. Nubia Sandstone overlain by shales are outcropping at the valley floor. A thick succession of sedimentary layers of Cretaceous / Eocene age, dominated by marine siliciclastic and carbonate deposits of the Nile Valley and Garra El-Arbain facies associations, is exposed along the eastern escarpment of the Kharga valley [1]. Karst phenomena (closed depressions, sinkholes, caves) can be observed within these lithologic units, most of them obviously created during more humid periods.

The Upper Cretaceous-Lower Tertiary sedimentary sequences overly nonconformably Precambrian basement rocks. The Neoproterozoic (900 - 550 Ma) basement in Central Egypt is dissected by intracratonic rifts and faults due to multiple episodes of geodynamic activity [6]. Older faults are predominantly E-W and NW, being intersected by younger N-E trending faults. Faults structures were re-activated by compressive forces from SE-NW and E-W directions. The tectonic setting of the Kharga valley is characterized by traces of these super-imposed E-W and N-S compressive forces [7]. In the Middle Tertiary further regional extensional forces appeared resulting in two complementary primary shear rifting system NW-SE (Red Sea or Gulf of Suez trend) and NNE-SSW [8]. The mostly E-W striking Nubian Fault System (NFS), that can be clearly mapped on satellite images, is extended from the Nile valley across the Kharga valley and the Western Desert. It is intersecting the Kharga valley with increasing density of the faults towards south. The E-W oriented fault zones are characterized by Late Cretaceous to present intra-plate strike-slip faults and fault related structures [9]. These faults have an influence on slope failure along the escarpments. Most larger mass movements along the eastern escarpments at the valley borders are concentrated in areas where active fault zones of the NFS are crossing the escarpments.

2. Materials and Methods

In the scope of this study evaluations are carried out based on open-source satellite data (Landsat, Sentinel 2, Sentinel 1 and ALOS PALSAR radar data), as well as on Google Earth and Bing Map high resolution satellite images. These evaluations of different satellite data were combined with available geodetic and geophysical data.

2.1. Optical Landsat, Sentinel 2 and World Imagery Data

The USGS Earth Explorer [10], the ESA Copernicus Browser [11], and NASA Earth Data [12] provided optical satellite data for this study. World Imagery-files from ESRI with high resolution satellite images were integrated into the GIS data base. The freely available Sentinel Application Platform (SNAP) / ESA and the commercial ENVI / NV5 Geospatial-Software were used for digital image processing, as well as the processing tools integrated into the geoinformation systems ArcGIS Pro / ESRI and QGIS.

Digital image processing of Landsat TM and 8 /9 (the Operational Land Imager (OLI), and Sentinel 2 data was focused on merging different Red Green Blue (RGB) band combinations, especially the creation of RGB images of the Landsat 8/9 thermal bands. Based on Sentinel 2 data the Modified Normalized Difference Water Index (MNDWI) was calculated that uses green and SWIR bands for the enhancement of soil moisture or vegetation water content: (MNDWI = (Green - SWIR) / (Green + SWIR). The MNDWI images provide information about soil and vegetation moisture in the Kharga valley.

Using the ERDAS software Principal Components image products were created by merging Landsat with SRTM DEM data. The processing strategy is as follows:

- The image was processed in ERDAS Imagine first as an 8-band layer stack (or composite band, for processing using the ATCOR-2 atmospheric correction plugin). It is important to know that ATCOR processing requires Landsat 8, Band 9, in the layer stack, hence an 8-band layer stack. Furthermore, all the bands are required to be in wavelength order, hence band layers become 1-5, 9, 6, 7.
- This layer stack was then processed using the RASTER/Spectral / Principal Component tool in Imagine.
- Combining DEM (hillshade) and Principal Component imagery: this is a simple, 2-band multiplicative calculation completed in Imagine using the Two Image Function routine. The rationale is to use this processing methodology to enhance the details of the surface landforms, specifically in arid landscapes - including scarps, structural controls and drainage, at all scales, in the processed satellite imagery. As this is the first study presenting this method, for the purpose of referencing this method, it is named the Hillshading Edge Enhancement Technique (HEET). The results are presented in section 4.2., Figure 13.

2.2. Evaluation of Satellite Radar Images

Radar signals, from satellite or airborne sensors, are radio waves, that when reflected from the Earth's surface, are returned as radar echoes, recorded and produced as a grayscale image, representing reflected signal intensity. Signals are transmitted in either vertical (V) or horizontal (H), (dual) polarisation, and are received as both vertical and horizontal waves by the satellite receiver. False colour composites are produced using a combination of

polarisations: VV, VH, HV, HH. The processing of the data was carried out using European Space Agency (ESA) SNAP software platform and ESRI ArcGIS Pro.

For this study, data from the following satellite systems were acquired from the following organisations:

- Sentinel 1 radar - European Space Agency (ESA): Synthetic Aperture Radar (SAR), C-band, 5.6cm wavelength [12]
- ALOS PALSAR – Nasa Earth Data and Alaska Satellite Facility (ASF): L-Band 23.5 cm wavelength [13]
- The Japanese Aerospace Exploration Agency (JAXA): ALOS PALSAR global mosaic and 12.5 m resolution PALSAR L-band data [14].

Long-wave radar data have proven to be very useful for geological studies as it has surface penetration capability of up to 2 metres in loose sediments very applicable for mapping drainage patterns [15].

2.3. Evaluations of DEM Data

DEM, Digital Elevation Model, represents digital surface topography derived from either SRTM of ASTER GDEM data available from the US Geological Survey [12]. SRTM is also available as clickable tiles from https://dwtkns.com/srtm30/. Using image processing / GIS software, ESRI ArcGIS Pro, QGIS and ERDAS Imagine, morphometric maps, such as slope, hillshade and drainage, and height levels can be produced with the aim of identifying landform features that may be associated with neotectonic movements [16] or provide hints about areas with exposure to slope failure.

2.4. Structural Evaluations

Faults, and fractures, dislocations with or without movements, in bedrocks are geological structure which are a potential risk to human infrastructure should they be subjected to the stress release of an earthquake. Faults and fractures are often expressed in imageries as a linear or curvi-linear feature – a lineament. However, other landform features such as valleys and scarps, depressions and drainage or vegetation and other geomorphological / geological features may also be identified as a lineament, as can pixels of similar color and greyscale tone. Mapping of lineaments from an image is either a visual and manual technique or derived from some form of algorithmic software. In this case a visual analysis was carried out as too many errors were expected using an automatic extraction because of longitudinal dune fields and linear, parallel wind erosion valleys, mainly in N-S direction. A statistical analysis of lineament orientations would not reflect the reality because of these reasons.

In risk mapping, active faulting is a significant feature to identify. Distinct visible displacements at the surface with only few traces of erosion support their detection. Another criterion is the occurrence of fault associated geological structures such as pull-apart basins and push-up ridges resulting from strike–slip related compression and stretching / releasing. These structures can be used to learn the relative age of the fault activity whenever the age of the outcropping rocks is known. Monitoring of movement by geodetic surveys [17] and the recording of earthquakes, current and historical are also important criteria to determine if a fault is active. Earthquake data were downloaded from [18], [19] and [20] and included into the GIS. When evaluating the satellite data the

following components were digitized: linear (lineaments) and structural features (synclines, anticlines, pull-apart depressions, push-up-ridges, take-off zones at cliffs).

3. Results

The presentations of the results are subdivided according to the different natural hazards.

3.1. Infrastructure and Agriculture prone to Aeolian Sediment Transport

Wind tunnel-like effects play an important role in the Kharga valley as they are concentrating and focusing winds from northern directions and increasing their intensity and wind speed, often resulting in dust- and sandstorms. The flat plateaus in the north are no hindrance for winds either. The wind tunnel-like effect supported the development of large, longitudinal dunes and of parallel dune fields with N-S orientation. The larger, longitudinal, often fixed dunes are covered by smaller, younger, active dune fields and sand sheets (Figures 3 and 4). Wind speed increases from November to January, reaching maxima from March to May causing even dust storms, such as "El-Khamasin" [21]. Local and supra-regional sandstorms crossing the area contribute to the deposit and sedimentation of extended, aeolian sand sheets. Parallel, N-S oriented stripes of aeolian sediments are clearly visible on satellite images. Besides the tectonic influence of N-S-oriented fault zones the Kharga valley in its longitudinal N-S outline is obviously the result of wind erosion as well, carving out parallel, smaller valleys and ridges.

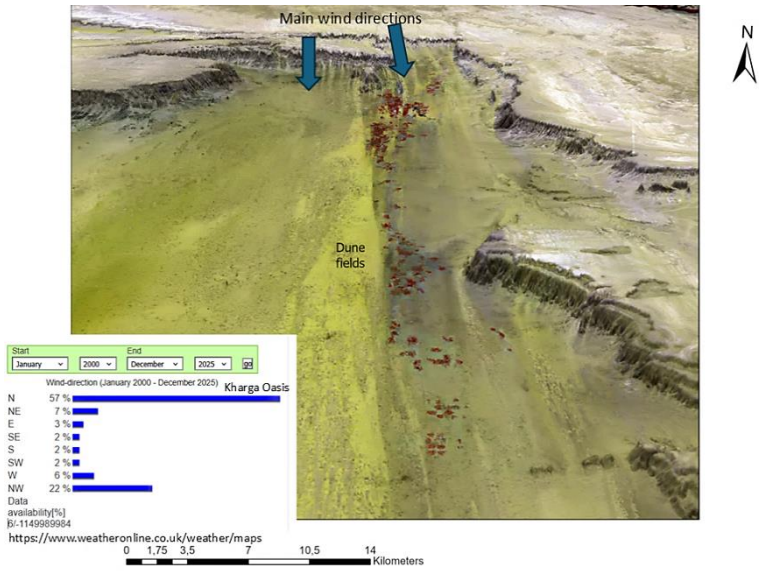

Figure 3. 3D perspective view of the northern Kharga valley visualizing the tunnel effect of the topography (10 x height amplification). The wind direction distribution data are available from [23]. The background Sentinel 2 mosaic was provided by [24].

These aeolian sediments form a risk for the infrastructure as they cover fields, settlements and roads. The development of this area is affected by the aeolian activity and requires measures such as adapting road routes to the movements of active dunes or as attempting to fix dunes. Their close monitoring (outline, thickness, movement) in time series is essential for land use planning. Wind corrosion, for example on historical buildings or irrigation machineries, can cause damage as well [25]. Figures 5 and 6 demonstrate the use of satellite images for

Mediterranean Journal of Basic and Applied Sciences (MJBAS)
Volume 9, Issue 4, Pages 179-206, October-December 2025

the inventory and monitoring of the activity of aeolian sedimentation. Figure 5 provides an example of active sand dunes covering roads (black arrows).

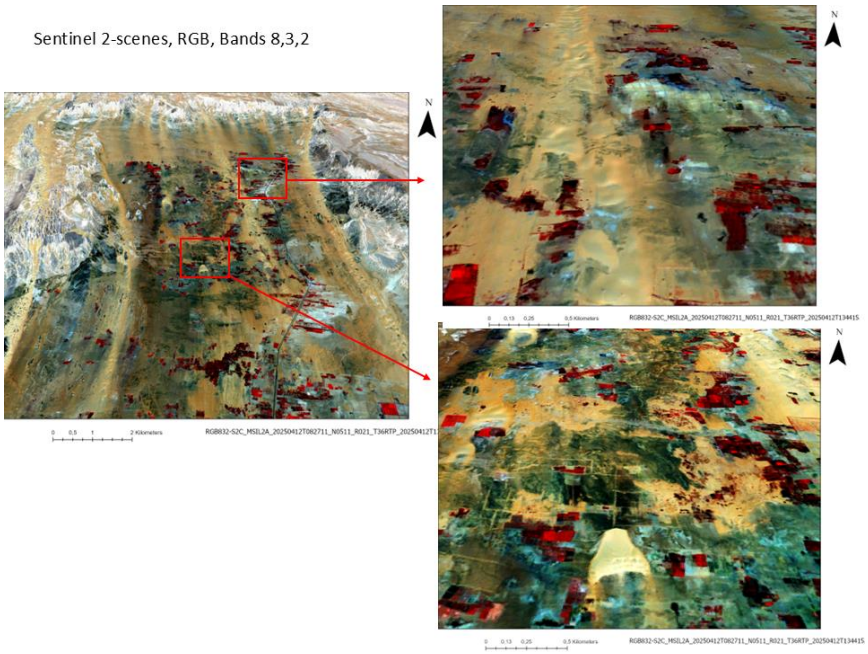

Figure 4. Sentinel 2 images (RGB, Band 8,3,2) in a 3D perspective view (5 x height amplification) of areas in the northern Kharga valley showing in brown-yellow colours the aeolian sediments, agricultural areas in red and green**.**

Figure 6 visualizes the development over 2 decades of El Kharga based on Google Earth scenes from 2003 to 2024. The growth of the settlements and agricultural areas was possible because of the availability of fossil groundwater in the Nubian sandstones. It appears that from 2003 to 2024 the position and outline of barchan dunes visible on the left side of the scenes (see blue arrows) have not changed noticeably on the satellite images, whereas the larger dunes at the center of Figure 6 are surrounded now by fields and are obviously fixed as far as possible.

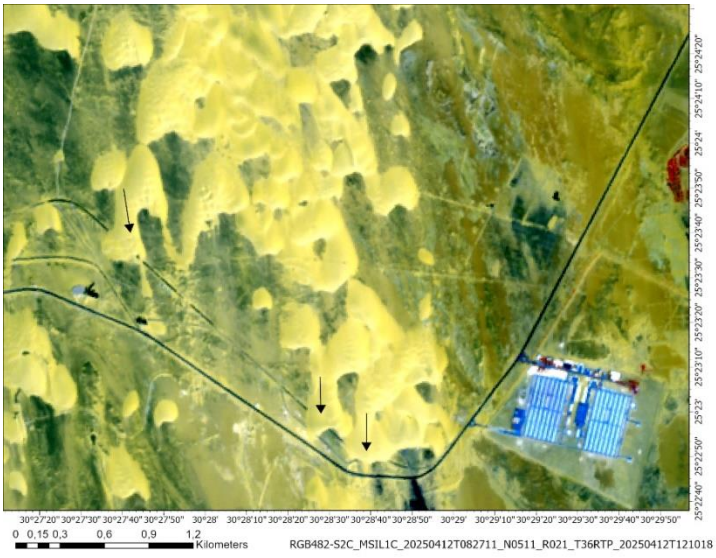

Figure 5. Aeolian sediments and barchan dunes covering roads (El Kharga-Asyut, 60) in the SW of El Kharga visible on a Sentinel 2 scene.

Mediterranean Journal of Basic and Applied Sciences (MJBAS)
Volume 9, Issue 4, Pages 179-206, October-December 2025

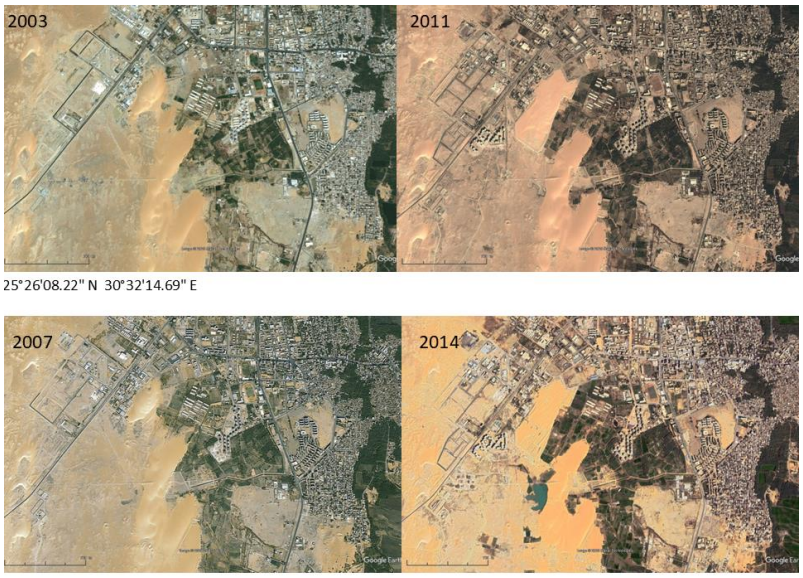

Figure 6. Google Earth time series (2003-2024) showing the growth of settlements and agricultural areas in El Kharga. Changes in the dune fields (blue arrows) are not visible during this time period.

3.2. Detection of Areas prone to Flash Floods

In the study area rare, locally higher precipitations that happen in decades (Figures 7 and 8) occur sometimes with relatively high rain intensities. Torrential rains have the potential to cause short-time flash floods in wadi paths that can affect the infrastructure in the Kharga valley. Although rain is very scarce, occasional rainstorms can affect the area, where rainwater can flow as sheet flash-floods, causing damage to villages and roads. The lowest areas < 40 m height level shows the highest probability to be exposed to flash floods, see the height level map (Figure 1). The absence of drainage outlets in the depression area and ridges of larger dunes forming barriers can augment the local impact of sudden, heavy rain clusters [22].

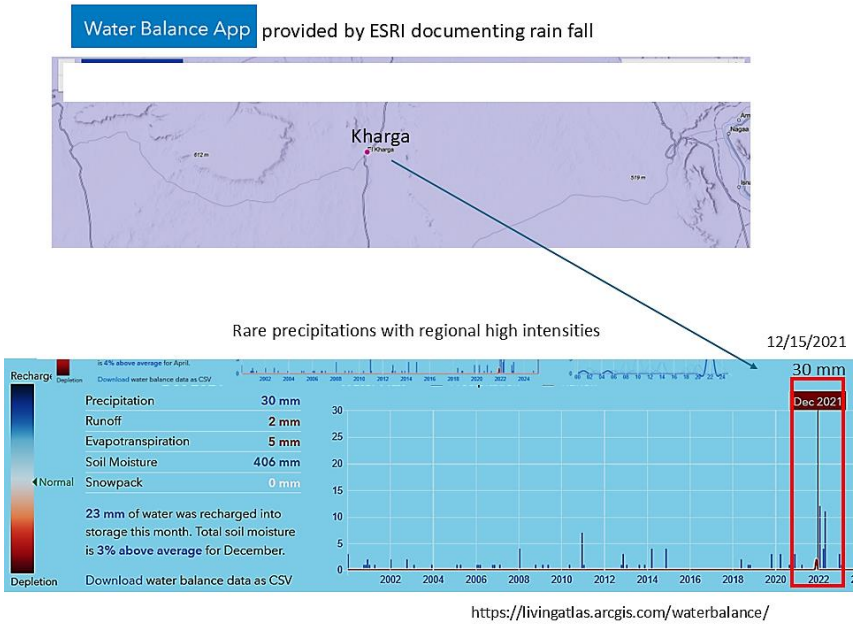

Figure 7. Rare rain fall events during the last decades with high precipitation intensities documented in the Water Balance App by ESRI [27].

Flash flood protection often relies on both: on structural measures like obstacle and detention dams to manage water flow and recharge groundwater, and on advanced forecasting and warning systems [26].

The amount and spatial distribution, especially clusters and concentrations of these precipitation events can be derived from satellite images, for example those provided by [27] and [28] (Figures 7 and 8). The close, continuous monitoring of clusters of these precipitation concentrations supports the preparedness for local flash floods.

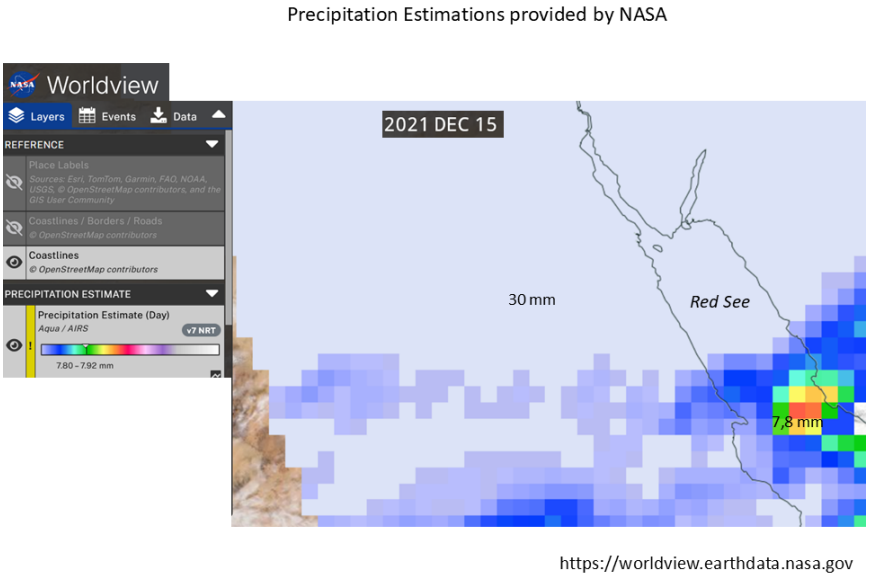

Figure 8. Estimated precipitations on 15.12.2021 by NASA, WorldView [28] and their spatial distribution.

Based on SRTM DEM data the drainage basins and stream order were calculated in ArcGIS Pro (Figure 9 a) to get an idea about the surface water catchment area in case of precipitations with high intensities. Considering the extent of the water catchment area for the Kharga valley (up to 200 km width and length) flash floods can be expected. However, the inhomogeneity of rain bearing clouds resulting in varying local rain intensities, the high evaporation, the infiltration into loose sedimentary covers, the karst hydrogeologic setting along the eastern valley border, dyke ridges and longitudinal dune ridges in the Western Desert building hindrances for run-off flow, etc., make the delineation of the flash flood prone areas a complex task. Most of them are concentrated in the lower areas, especially to areas below 40 m height level (dark-blue and < 20 m - violet in Figure 9 a).

Flash floods are generally following already existing drainage networks. Thus, the analysis of the existing dry riverbeds and the dry drainage network is important for land use planning to avoid flooding of settlements and agricultural areas in case of intense rain clusters. As constructing flood prevention dams is one option for flash flood protection, it is important to recognize sites for successful dam construction, or for construction of detention basins for water harvesting. Fresh water harvesting in the time of these rare precipitations in more detention basins might be a possibility. Further on, the knowledge of sites, where infiltration of surface water predominantly occurs, supports the exploration of groundwater bearing zones. This knowledge was obviously used in the historic past: Following the discoveries made in Dakhla during the Dakhla Oasis Project, a large system of qanats was identified at Dush, in the south of the Kharga depression [29].

Mediterranean Journal of Basic and Applied Sciences (MJBAS)
Volume 9, Issue 4, Pages 179-206, October-December 2025

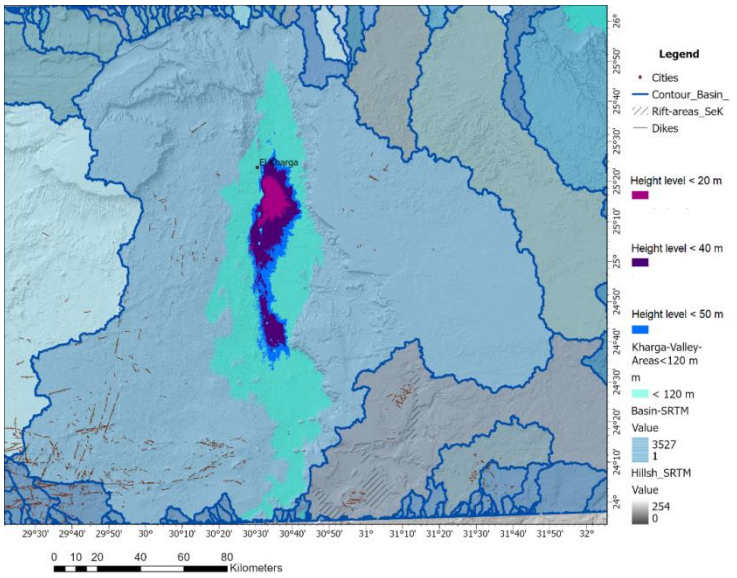

(a)

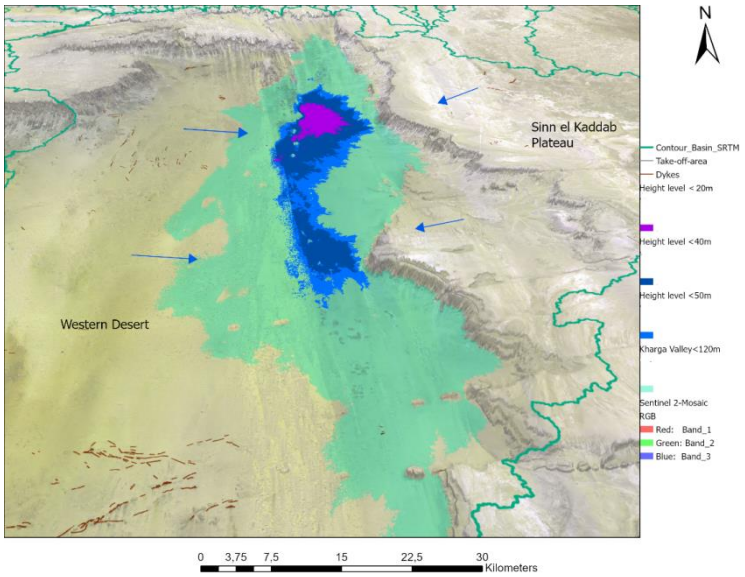

(b)

Figure 9 a and b. (a) Drainage basins (outline – blue lines) in the Kharga valley (green) area, (b) 3D perspective view visualizing the flow direction (blue arrows) into the lowest areas (dark-blue, violet).

Examples of the remote sensing contributions are presented in the next figures. Traces of rare rain events can be clearly detected especially on radar, Landsat and Sentinel 2 images by revealing past drainage patterns. Knowing these drainage patterns and the main flow paths is important for avoiding damage in case of flash floods. Traces of the water discharge caused by difference in the elevations at the valley border and the elevation of the valley bottom where the discharge is directed, are clearly visible on the satellite images (Figure 10). Wadi beds provided a pathway for stones, gravel and sand shaping an alluvial fan. The fan-shaped drainage beds are covered in the west by large dune fields. Surface water infiltrating into the loose sedimentary covers after rare rains is relatively "protected" after infiltration against evaporation to a varying extent by these large dune fields and aeolian sand sheets in the west (Figure 10 a). The RGB radar scenes created based on different polarizations (Figure 10, b) and

(d)) enhance subtle differences in the streaming pattern due to variations of the radar reflection. Coarse grained surface material caused a relatively stronger radar reflection, thus, is appearing in lighter colors within the alluvial fan (Figure 10 d).

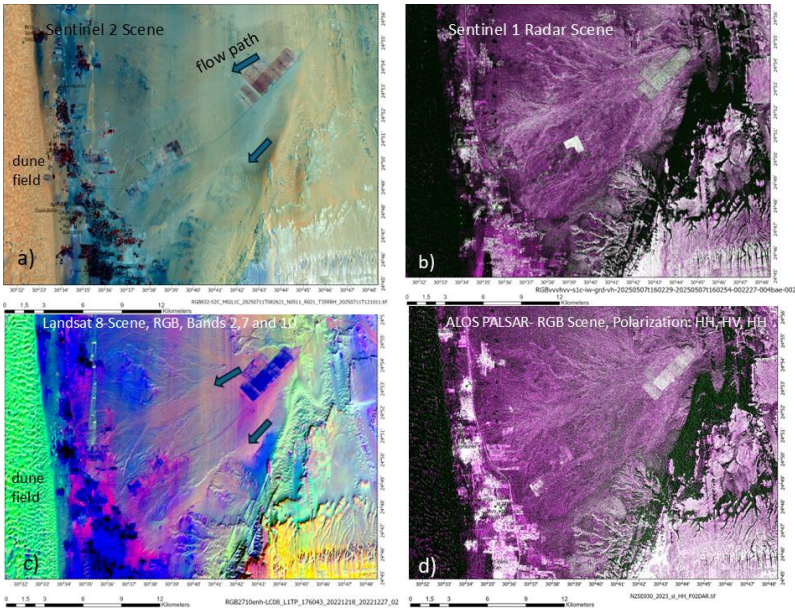

Figure 10. Sediment flow visible on satellite images a) Sentinel 2-scene, b) Sentinel 1-radar scene, c) Landsat scene, and d) ALOS PALSAR radar scene.

On Figure 11 traces of past surface water flow are visible on the different optical and radar satellite images. They are exactly directed towards the settlement on the left side of Figure 11. The Landsat scene (c) shows the wadi beds in orange colors.

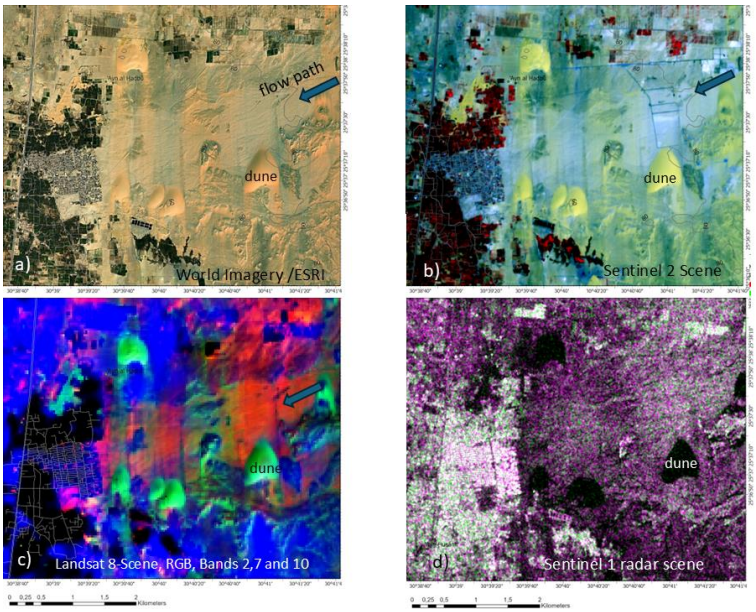

Figure 11. Surface water and sediment flow beds from the eastern valley rim towards the valley bottom, later covered by aeolian sediments, a) World Imagery-file / ESRI, b) Sentinel 2-scene, c) Landsat-scene, wadi beds-orange, dunes – green, d) Sentinel 1-RGB-radar scene. The drainage beds are still clearly visible on the Landsat scene underneath the aeolian covers.

Mediterranean Journal of Basic and Applied Sciences (MJBAS)
Volume 9, Issue 4, Pages 179-206, October-December 2025

The next Figure 12 visualizes in another example that the comparative analysis of different satellite images helps to locate flow paths. The Landsat scene (RGB, combining the bands 2,7 and 10, c) on Figure 12) shows the wadi beds again in orange colors. The Modified Normalized Difference Water Index (MNDWI)- scene derived from Sentinel 2 data (b) on Figure 12) allows the detection of wadi beds even beneath aeolian covers as well. The Sentinel 1 radar scene (d) enhances the streaming pattern. This knowledge might support not only flash flood preparedness, but also the search for locations of wells. It can be useful for water harvesting in this area (Figure 12 e) whenever wadi beds or depressions are filled temporarily with water after heavy rains. Planning of smaller water detention basins might be a possibility to preserve water after rare rainfall.

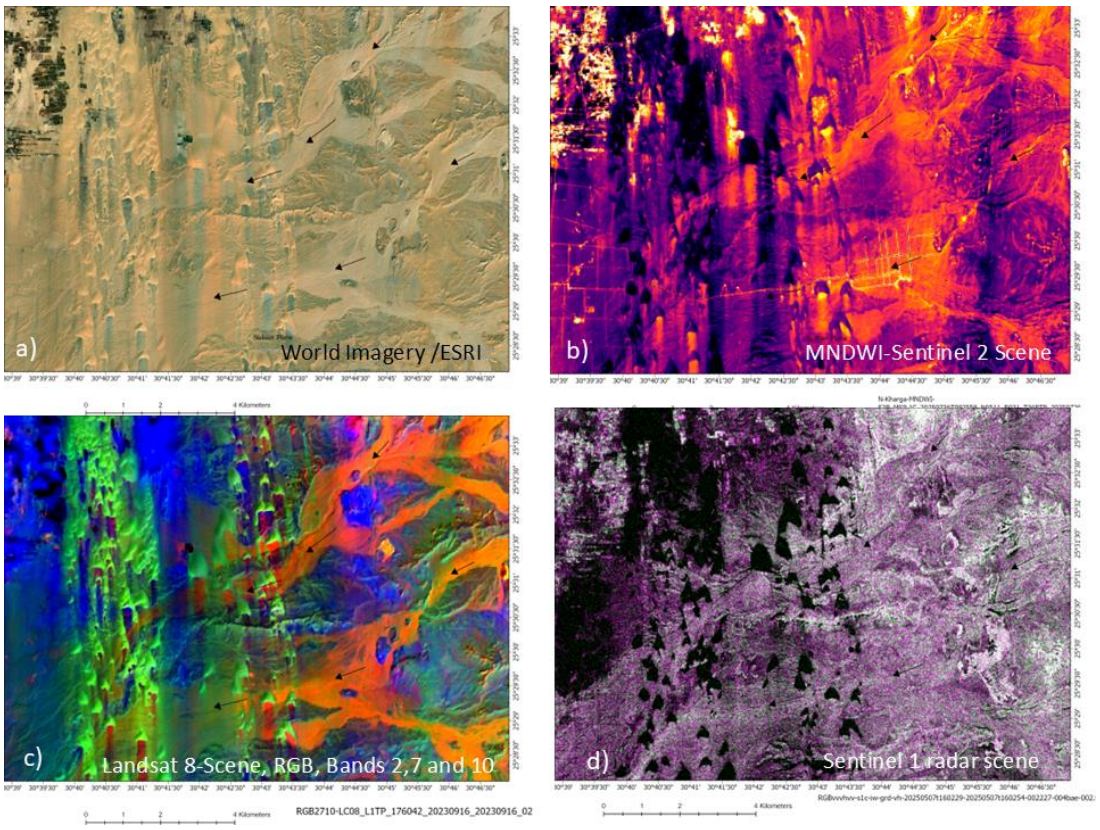

(a-d)

(e)

Figure 12. Drainage network covered by dune fields. (a) World Imagery-file / ESRI, (b) Sentinel 2- MNDWI image, (c) Landsat-scene, (d) Sentinel 1-radar scene, (e) water filled basins after heavy rains suited for water harvesting (Field image of an example of a short-term rain water filled depression: Theilen-Willige, 2020).

The result of the Principal Component Analysis (PCA) of Landsat data combined with a SRTM hillside map is presented in Figure 13. This image is created using the Hillshade Edge Enhancement Technique explained in

Section 3.1. The band combinations are of: RGB PC3, PC2, PC1 identifying drainage coming off the escarpment into 2 wide channels, in blue, which can be detected spreading out onto the valley center beneath the barchan sand dune cover.

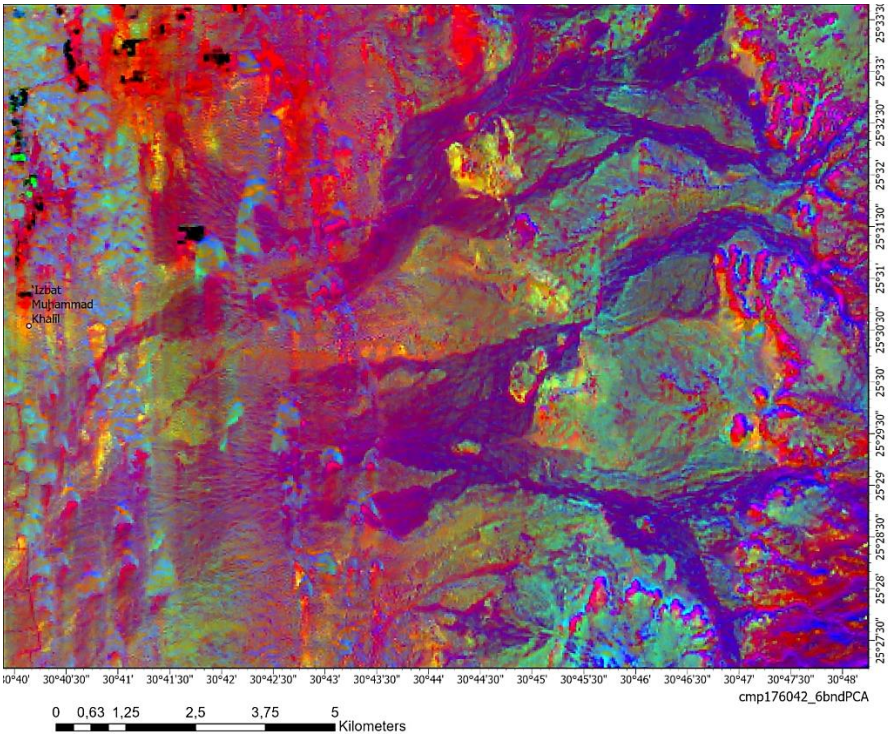

Figure 13. Principal Component Analysis (PCA) of Landsat data combined with the Hillshade Edge Enhancement Technique (HEET) created by E.A.Dubowski.

3.3. Mass Movements

Traces of several types of slope failure can be detected on high resolution satellite images along the steep escarpments at the borders of the Kharga valley. Mass movements are dominated by sediment transport from the escarpments toward the valley center. The finer-grained material is reactivated again by wind transport providing material for aeolian sand sheets and dunes. Following types of slope failure are prevailing. Block-wise displacements of larger rock units, block gliding and rotation, rockfall and debris flow (the latter after rare rainfall events). The material transported from the escarpments downwards to the valley bottom forms thick sediment layers. As mass movements because of slope failure and erosion / sedimentation from the valley borders are directed towards the valley center, where settlements and agriculture are concentrated, their monitoring is essential. Height differences influence the intensity of sediment transport:

In the northern part of the Kharga valley, the height differences between the escarpments on both sides and the valley bottom amount up to 500 m leading to intense morphodynamical processes (Figure 14 a). In the middle part of the Kharga valley the height differences between the eastern escarpment and the valley center decrease to about 400 m (Figure 14 b and in the southern part to 300 m (Figure 14 c). The valley width decreases from N to S as well from about 50 km near El Kharga to 25 km in the southern part. With less height differences and width, the sediments transport appears reduced on the satellite images in comparison with the northern part of the valley.

Mediterranean Journal of Basic and Applied Sciences (MJBAS)
Volume 9, Issue 4, Pages 179-206, October-December 2025

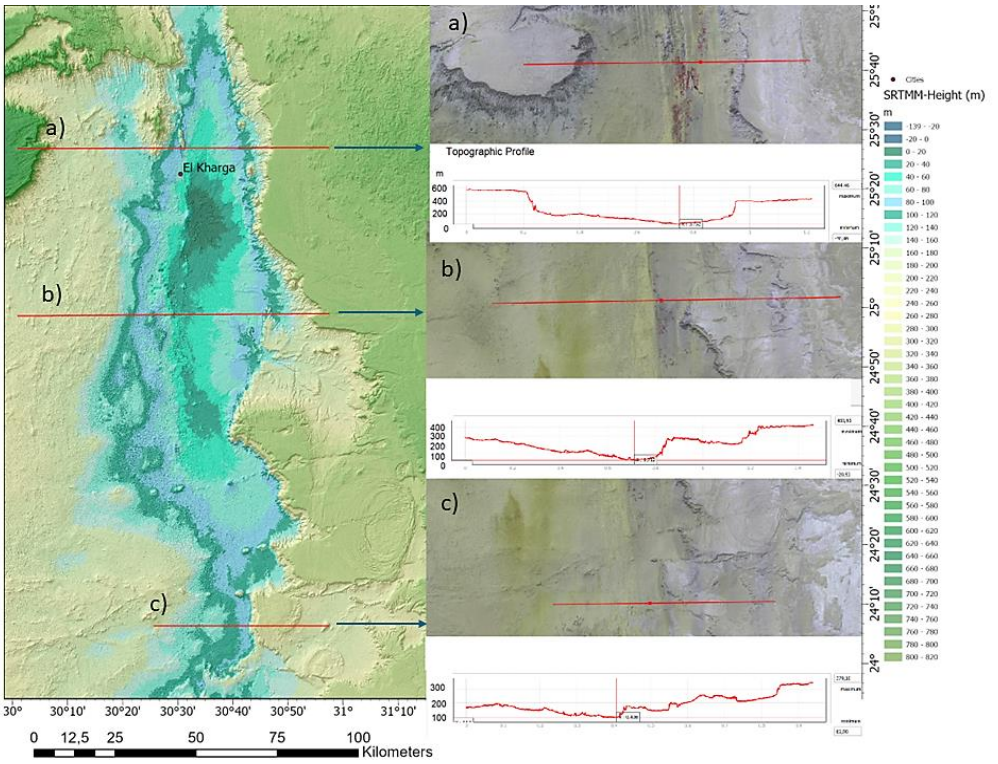

Figure 14 a-c. Topographic E-W-cross sections along the Kharga valley.

Figure 15 shows a classification result based on Sentinel 2 data from the northern Kharga valley. Wadi beds become clearly visible in dark-blue colors. The Sentinel 2-scene of this area visualizes the areas of erosion and sedimentation within broader valleys (blue in Figure 15) in case of precipitations.

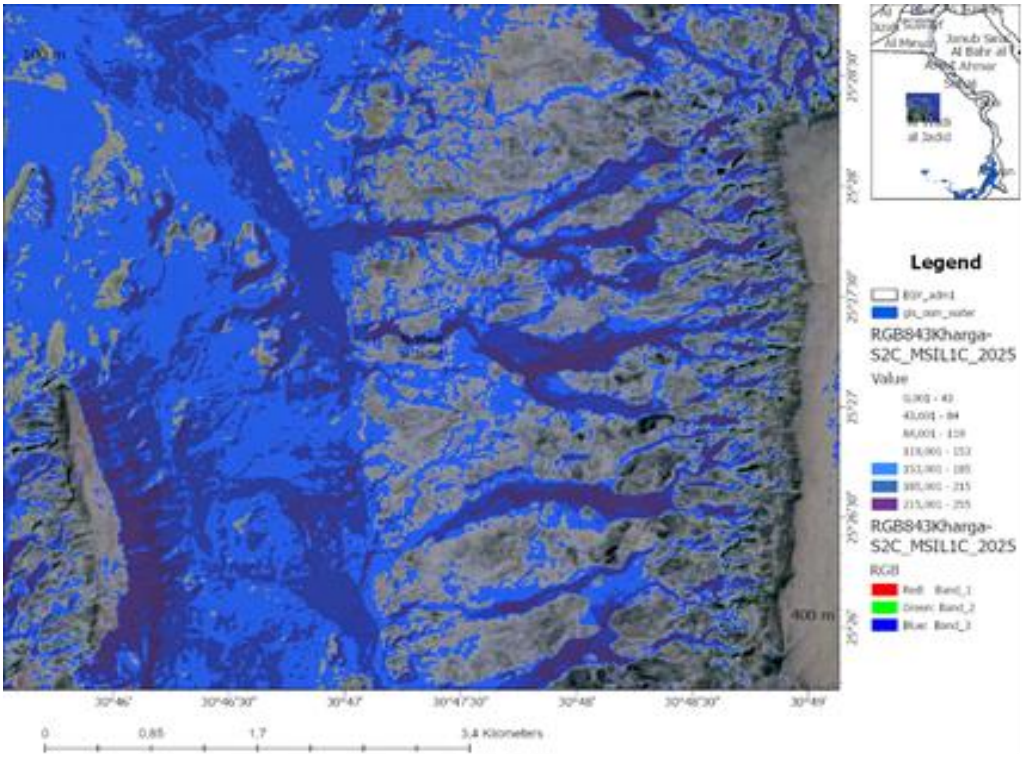

Figure 15. Fluvial erosion and aeolian and fluvial sedimentation areas (blue) along the eastern Kharga valley rim visible on a classified Sentinel 2 scene.

Figure 16 provides an overview of areas with slope degrees larger than 50° (derived from SRTM DEM data) as steep slopes generally show a higher susceptibility to slope failure. The observed areas with detected slope failures on high resolution satellite images, most of them rock fall and block-wise movements, were digitized. Earthquake epicenters were included as well. Stronger earthquakes have the potential to trigger mass movements.

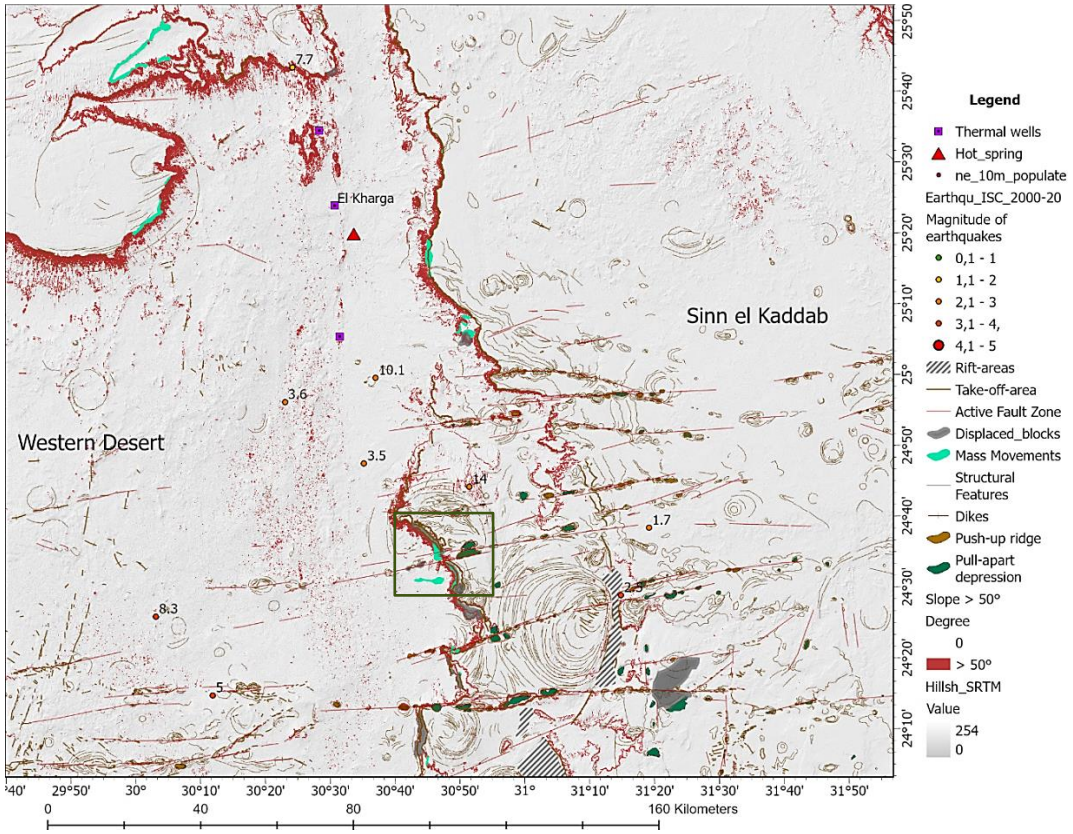

Figure 16. Overview of areas with steep slopes (> 50°) and observed mass movements (green) along the escarpments. The next Figure 17 shows an amplification of the indicated area (rectangle).

Figure 17 shows in a perspective 3D view a Sentinel 2 scene of the eastern valley border indicating areas with block-wise movements and smaller block-gliding. Larger, elongated displaced blocks can be observed as demonstrated by Figure 18, especially in areas where large fault zones are intersecting the cliff sites. After the separation along crown cracks and fault zones, slope parallel, larger blocks moved downwards, resulting in a narrow valley between the crown of the crown of the cliff and the dislocated block. The separation is indicated by the congruent, “zipper-like” outline of the eastern rim of the block and the western rim of the cliff. Whether these block movements are recent or are paleo-landslides, or both, and reactivated, this cannot be determined based on remotes sensing data. Field work is necessary to solve the questions related to their origins. In case of stronger earthquakes movements of such larger, dislocated blocks could be triggered or increased. Further cracks and fissures at the crowns of the escarpments might open as demonstrated in Figure 19. The structural stability of the cliffs is weakened whenever tension cracks widen and deepen, then causing the surrounding rock to fail and collapse. The monitoring of those cracks, fissures and take-off zones along the cliffs is an important part of hazard preparedness. Block displacements and mass movements can be used as indicators for neotectonic activities as well when observed and documented continuously and combined with geodetic and field measurements.

Mediterranean Journal of Basic and Applied Sciences (MJBAS)
Volume 9, Issue 4, Pages 179-206, October-December 2025

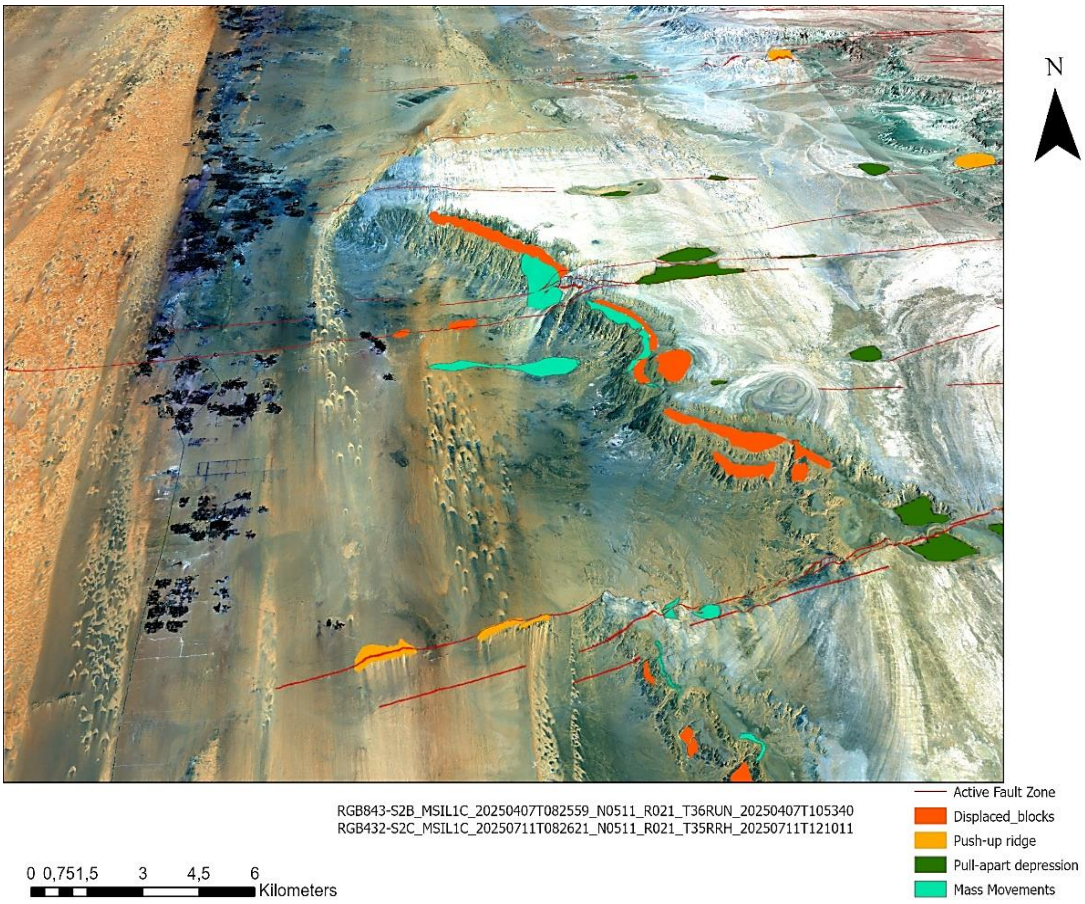

Figure 17. Steep slopes with visible slope failures on a Sentinel 2 - 3D perspective view in the southern part of the Kharga valley (5 x height amplification).

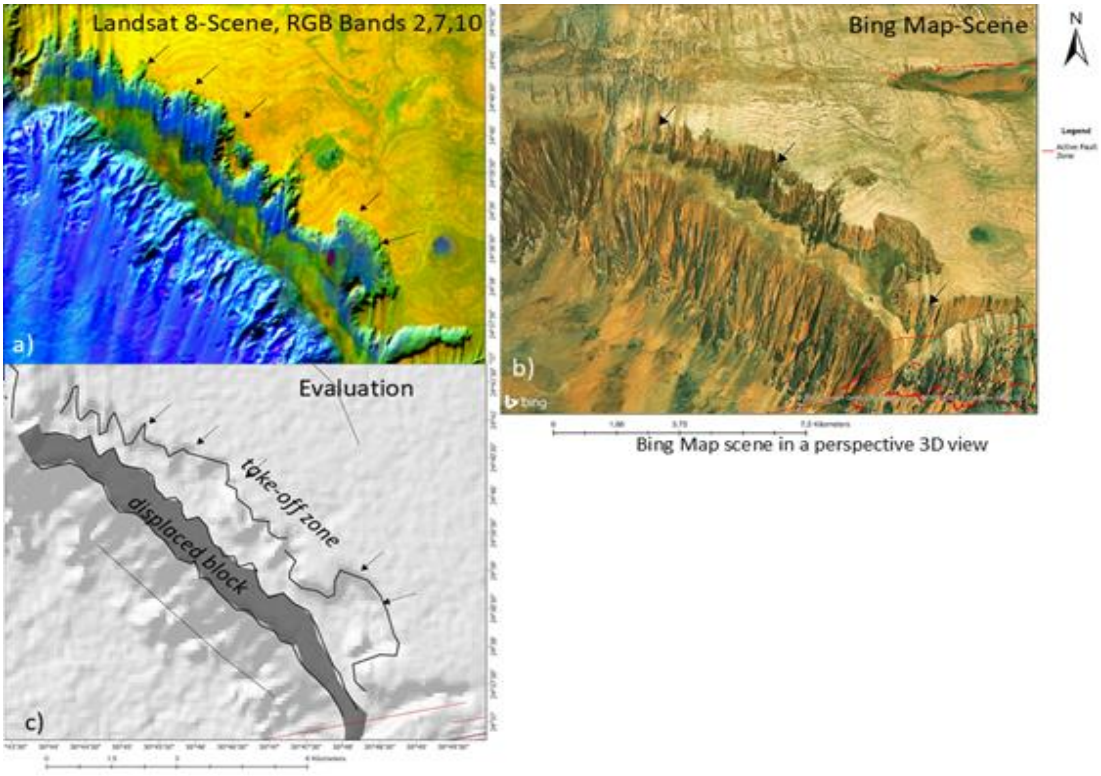

Figure 18. Displacement of larger blocks visible on a) Landsat 8, b) Bing Map-scene, and c) the evaluation.

Mediterranean Journal of Basic and Applied Sciences (MJBAS)
Volume 9, Issue 4, Pages 179-206, October-December 2025

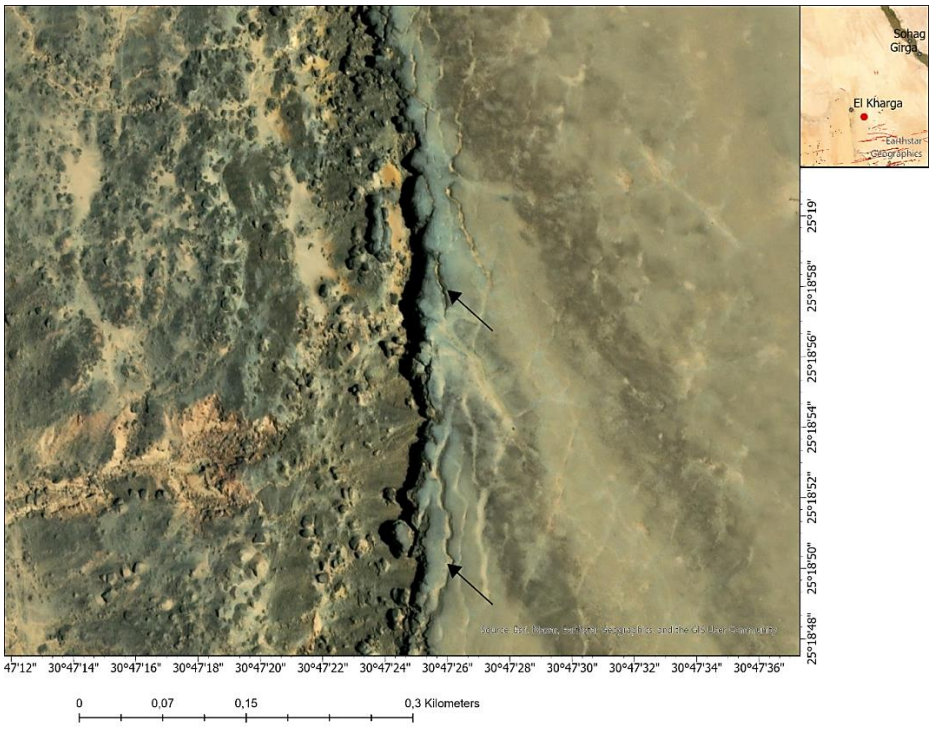

Figure 19. Fissures, opening cracks (black arrow) and block-gliding along the main scarps visible on a World Imagery-scene. On the flat top surface of the cliff, tension cracks run parallel to the cliff face.

The development of the N-S oriented, linear escarpment at the eastern border of the Kharga valley was obviously influenced by fault zones with the same orientation.

3.4. Geodynamic Activities

Part of the geodynamic activities are seismic and aseismic movements in the Kharga valley area. Evaluations of the different satellite images reveal traces of intense geodynamic activities in the past up to present. The position of active fault zones in the Kharga valley, that are often covered and buried by younger aeolian and fluvial sediments, can be derived partly by the evaluations of radar images with penetration capabilities of radar signals into loose, unconsolidated sediments. Some of them are still visible on the ALOS PALSAR radar images because of the penetration capabilities of the long-wave radar signals. Radar images reveal distinct E-W-oriented linear features that trace the faults underneath. Hidden fault segments can be detected on L-Band radar images whenever they are in the range of long-wave radar penetration. Experiments of [30] have delivered a potential explanation besides radar penetration: The visibility of linear features within aeolian sediments and dune fields on radar images might be explained by fabric reorganization within so-called disaggregation bands. They are formed in unconsolidated sediments above faults when shear stresses from the active fault rotate the unconsolidated grains, causing them to slide against and past each other. This process also leads to a reduction of pore space.

Earthquake epicenters are included in Figures 20, combined with known active faults and visual lineament analysis derived from satellite image evaluations. Fault zones with mainly E-W- orientation belonging to the Nubian Fault System (NFS), characterized by strike-slip faults [32] and fault related structures such as pull-apart depressions, push-up ridges and rotation structures, can be detected on the satellite images as well as traces of N-

S, SW-NE and SE-NW fault systems (Figures 20, 21). The distribution of the main orientations of visible active faults is presented in a rose diagram (Figure 20 b). Traces of larger rotation structures visible in the Tertiary clay, marl, lime- and dolostone of the Sinn el Kaddab plateau appear concentrated along the eastern border of the Kharga valley.

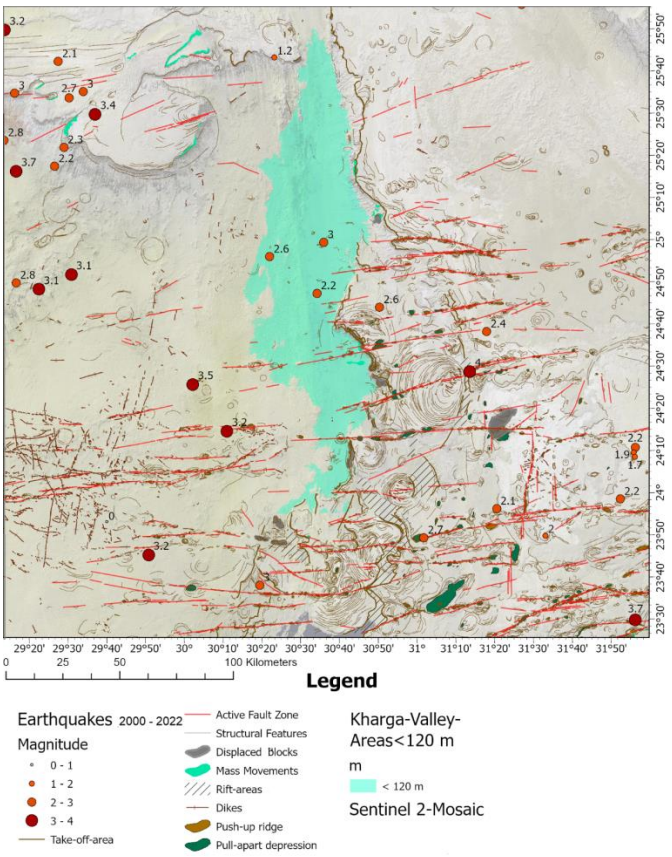

(a)

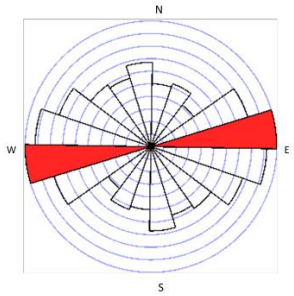

(b)

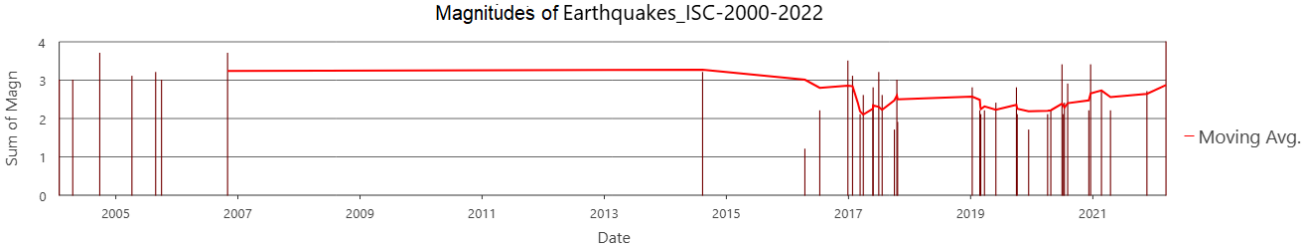

(c)

Mediterranean Journal of Basic and Applied Sciences (MJBAS)
Volume 9, Issue 4, Pages 179-206, October-December 2025

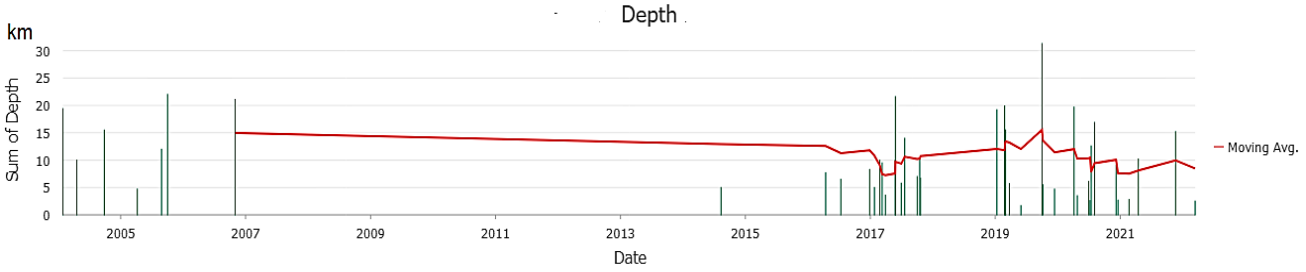

(d)

Figure 20. Overview map of active fault zones, structures and earthquakes in the Kharga valley area, (a) overview map of earthquakes from 2000-2022, (b) line direction histogram of visible "Active Fault Zones" including percentage circles and trends (red), (c) magnitudes of these earthquakes, (d) depths of these earthquakes. The earthquake data were downloaded from [20].

Earthquakes, or seismic movements, are not the only ways active faults respond to shear stresses. Slow, long-term creep, aseismic movements accumulate over time. Fault zone instability associated with this aseismic activity is a stability issue for human infrastructures [31], and hence, should be taken into account as a significant risk factor.

Most of the documented earthquakes [20] in the Kharga valley show a diffuse spatial pattern and magnitudes up to 4 (Figure 20 a and b). It seems that earthquakes occur in timely clusters. Their depths vary between < 5 to > 30 km (Figure.20 c). These earthquake data covering only a relatively short time period are not sufficient to allow a reliable statistical analysis. The effects of far-field earthquakes within longer distances from the Kharga valley with magnitudes > 4 should be considered as well.

Local site conditions (for example outcropping loose sands or rocks) influencing shear wave velocities play an important role with respect to potential damage due to varying intensities and duration of earthquake shock. There have been no published investigations in the study area dealing with this aspect so far. Secondary effects related to higher earthquakes shock and stronger ground motion (such as slope failure, compaction of loose, sedimentary covers, vertical or horizontal displacements along faults) have to be included into the hazard monitoring system as areas susceptible to those effects should be known. Towards the center of the Kharga valley the fault systems are buried underneath younger, loose, unconsolidated sediments (Figures 21 and 22). So far, no information is available regarding the influence of neotectonic movements or of secondary effects of earthquakes on the infrastructure such as on piping systems. However, it can be expected that after stronger earthquakes secondary effects like compaction of the ground might occur. There is no information of local site conditions publicly available.

The parallel, nearly equidistant, linear drainage segments, and the fluvial sedimentation and erosion pattern in E-W direction indicate not only gravitational, but also a structural influence on their shape and orientation, and very likely are influenced by recent movements.

When analyzing combined height and radar data it seems that the area of the Kharga valley might be prone to compression and vertical movements (uplift, subsidence) due to geodynamic, intra-plate tectonic stress. Figure 23 shows a topographic N-S-profile indicating undulating valleys and hills oriented in E-W-direction.

Amplifying the height (10 x), 3D perspective views of a Sentinel 1 RGB radar image clearly trace these linear, parallel valleys and hills (Figure 24). Further research is needed to explain these surface features and their structural setting as it is important to know the critical areas for the maintenance of the infrastructure, especially in zones with contrary movements.

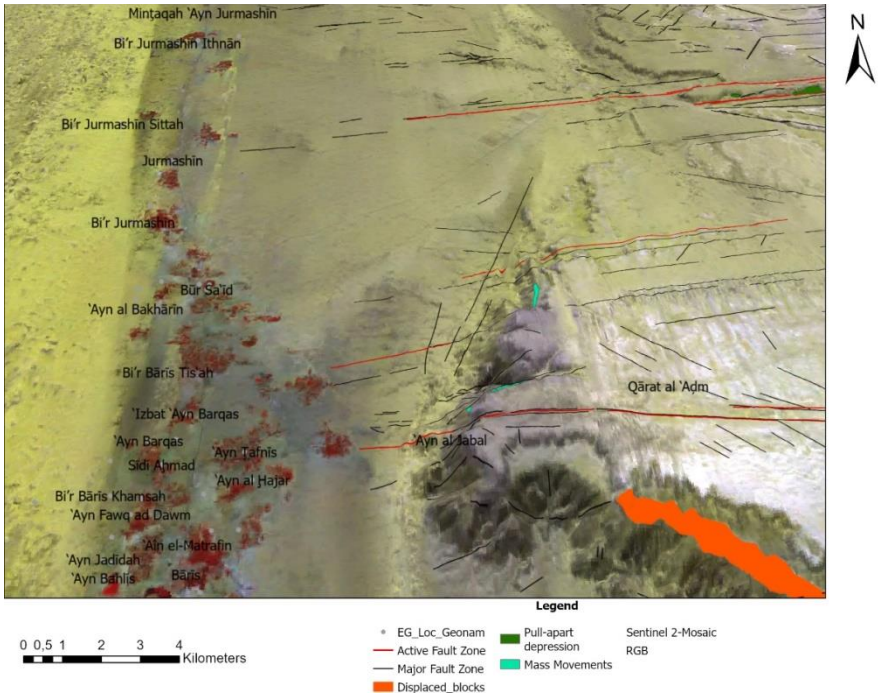

Figure 21. Perspective 3D view of a Sentinel 2 scene indicating clearly detectable fault zones at the eastern border of the Kharga valley. Settlements and agricultural areas are visible in red.

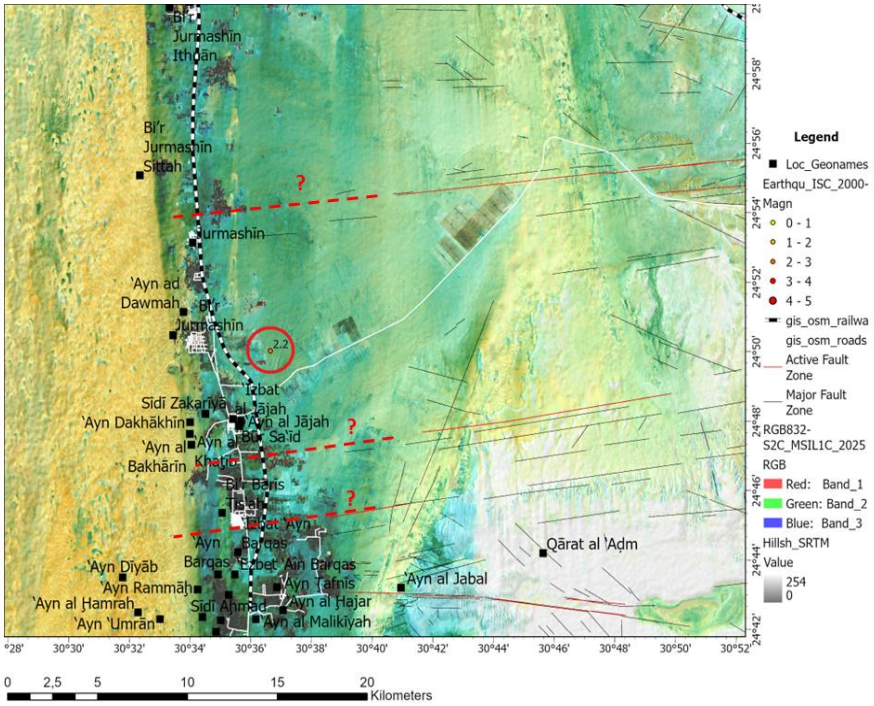

Figure 22. Lineament analysis for the detection of fault zones (red lines) buried underneath loose, unconsolidated sediments at the valley center.

Mediterranean Journal of Basic and Applied Sciences (MJBAS)
Volume 9, Issue 4, Pages 179-206, October-December 2025

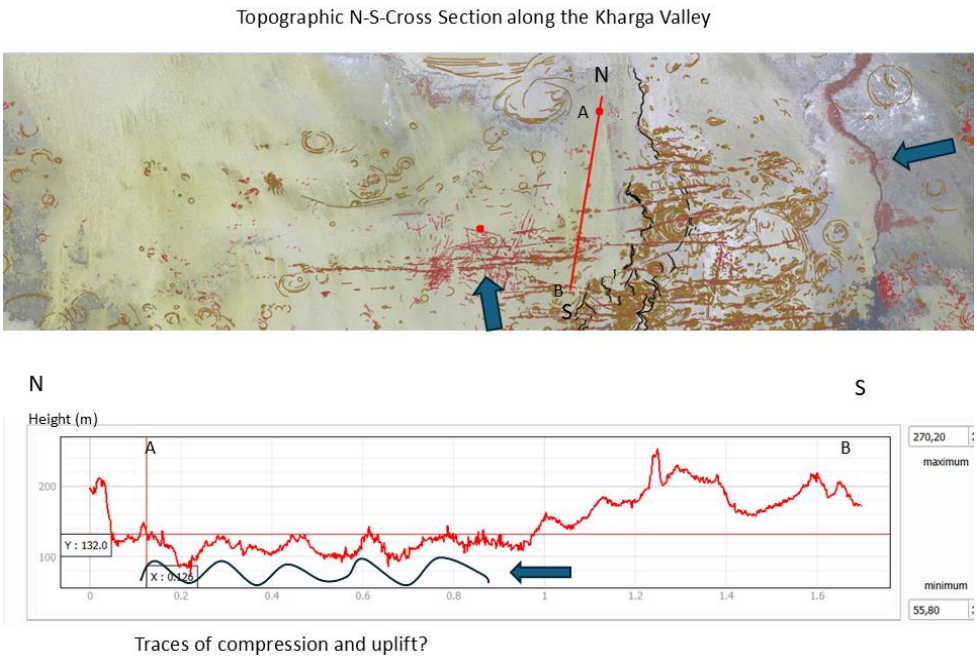

Figure 23. N-S topographic profile along the central-Kharga valley. The blue arrows symbolize the main stress directions.

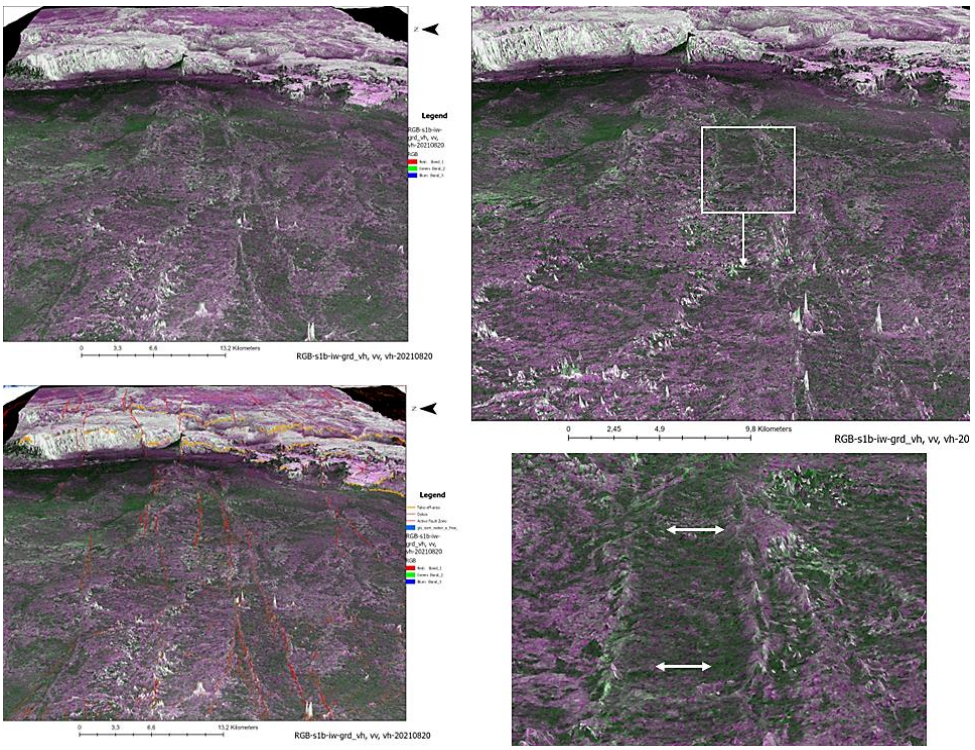

Figure 24. Structural influence on surface topography, a) 3D perspective view of a RGB-Sentinel 1 radar image of the central Kharga valley looking towards east, b) mapping of fault zones (red lines), c and d) amplifications of the radar scene visualizing linear valleys and hills with E-W-orientation.

3.5. Karst

The tectonic/geodynamic situation is affecting the groundwater setting in this area such as by influencing the development of the karst hydrogeologic network, and the hydraulic gradient as well as the permeability of the

rocks. As the limestones in the Sinn el Kaddab plateau have been affected by intense tectonic stress (due to uplifting, movements along active fault zones, or rotation) during the geologic past, the rock units have been fractured and dislocated. Nowadays, rare rainwater from the higher areas in the Sinn el Kaddab plateau can infiltrate into these fracture and fault zones and into a complex, karst hydrogeologic underground conduit system within the lime-and dolostones. Groundwater and surface water exchange with both adjacent and distant aquifers through underground channels can be expected. Following the hydraulic gradient, groundwater is partly flowing towards west into the Kharga valley.

As the Kharga valley is bordered by outcrops of marls, lime- and dolostone sequences along the escarpments, their hazard potential for this area comprises mainly mass movements as shown in the Section 3.3.

4. Discussion

The presented examples of the use of satellite data and their evaluations in a GIS embedded environment have clearly demonstrated their value for natural hazard assessment and a GIS integrated data mining. However, information gained from processed satellite data can only be one step and layer in a mosaic of monitoring systems.

- More detailed ground truth works and data integration are needed. Research gaps are revealed such as for example: for the monitoring of the aeolian activities more meteorological data are needed such as wind speed, level and intensity combined with detailed aeolian sand load and transport velocities monitoring.

- For the earthquake hazard assessment more geotechnical field work is needed in this area to get more detailed knowledge about the local site conditions in the Kharga valley in case of stronger earthquakes.

- Based on the different satellite images the mapping of linear features related to fault and fracture zones could be carried out and, thus, contribute to the inventory of existing and potential active fault zones. But more detailed knowledge is necessary to answer open questions related to recent movements along the fault zones and their impact on the formation of fault related structures. For the maintenance of the infrastructure it is important to know how far active are strike-slip faults intersecting the valley. Geodetic data would support the detection of aseismic, long-term movements.

- Could movements along the NFS fault system influence the artesian groundwater flow conditions? The surface water input along the fault zones within the Sinn el Kaddab plateau with karst hydrogeologic conditions flowing towards the Kharga valley is another research theme that should be investigated more detailed.

5. Conclusions

Several natural hazards were described in the investigation area affecting the economic development, maintenance of the infrastructure and the safety of settlement using satellite and additional geodata integrated and evaluated in a GIS environment. The monitoring of aeolian activities, especially of active dunes, of flow paths in case of flash floods, of mass movements along the escarpments, and sediment erosion and deposition within the valley, of aseismic geodynamic activities along fault zones or earthquake shock and secondary effects related to earthquakes, supports the development and the planning of protection measurements such as storage and

retardation dams or wind protection. Without consideration of wadi paths that lead surface water flow in case of rare local, heavy precipitation cells, flooding of agricultural areas, settlements or of infrastructure can be expected.

This is demonstrated by Figure 25 showing railroad segments prone to aeolian activities and to flashfloods in case of sudden, heavy rains.

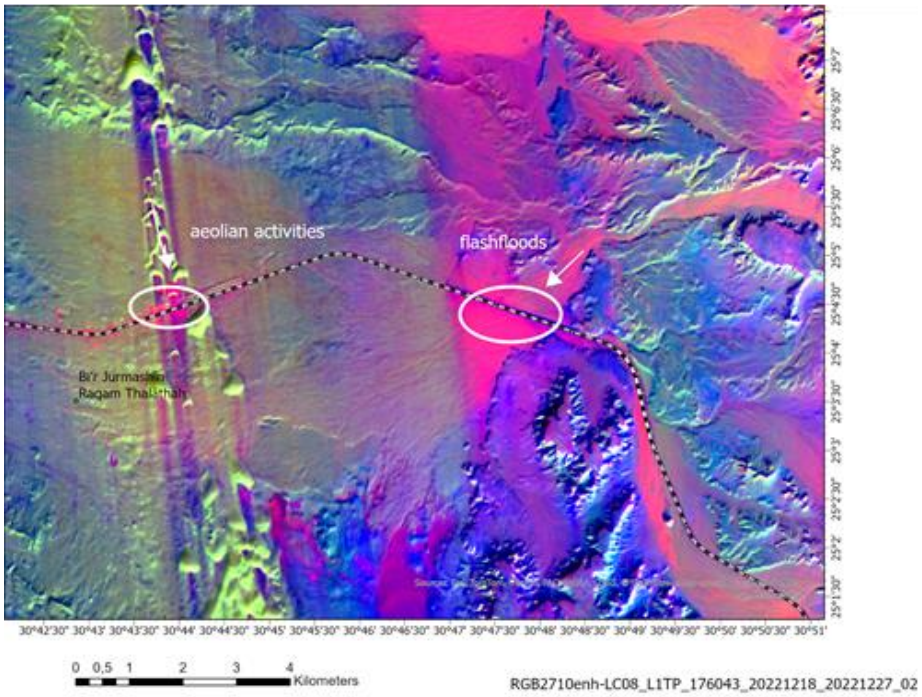

Figure 25. Landsat scene (RGB, Bands 2,7 and 10) showing railroad segments affected by aeolian activities and in case of heavy rains by flash floods. Flash floods might be concentrated by the narrow, uphill flow path. The railroad-shape file was downloaded from [33].

It can be stated that the combined evaluations of different satellite data are helpful to localize and monitor critical areas exposed to different natural hazards.

- Landsat RGB combining thermal bands and PCA images have shown their value for the detection of wadi beds exposed to flash floods in case of heavy rains, as well as the MNDWI water index image products derived from Landsat and Sentinel 2 data. The position of the construction of hydraulic structures like storage dams, cisterns, and retardation dams that are an important part of the catalogue of damage prevention measures [34], can be planned more precisely when considering these findings.

- From radar data structural and fault information can be gained that are not often visible on optical satellite images because of the sedimentary covers, but are essential for seismic hazard preparedness. The structural setting influences the local site conditions (ground motion differences because of reflections or guided seismic waves along fault zones) and earthquake related secondary effects (compaction, horizontal/vertical movements). Whenever planning, for example piping systems, this knowledge should be considered.

- Creating maps with areas prone to mass movements or to flooding is a basic prerequisite for initiating and planning further research. It requires time-consuming, experienced analyzing work using different satellite data

including the testing of the best suited digital image processing methods. High resolution satellite images support the detection of opening cracks and fissures along the escarpments leading to further block movements.

- Remote sensing data embedded in GIS environment form important layers in a natural hazard information system. The results derived from the evaluations of remote sensing data could support decision-makers, as based on the gathered data specific adapted strategies and plans for damage mitigation and prevention can be developed [35]. Thus, beyond hazard assessment and monitoring, GIS and remote sensing could contribute to long-term resilience building.

- Adequately flexible mechanisms for handling hazards such as building an effective communication network with all parties concerned dealing with the disaster can be implemented. Engaging all associations as well as government and non-government organizations to develop the necessary organizational frameworks is important [36].

- Data mining based on satellite data, different geodata and field data as demonstrated in this study are the prerequisite for the future use of Artificial intelligence (AI) that offers advanced machine learning techniques to analyze vast datasets, improving prediction accuracy, supporting early warnings, and emergency response. The challenge is obtaining a sufficiently large and representative set of training data [37]. To benefit from the advantages of AI and to train AI a reliable basic data set and long-term monitoring of the different types of natural hazards in the Kharga valley is necessary to avoid AI errors.

Declarations

Source of Funding

This research did not benefit from grant from any non-profit, public or commercial funding agency.

Competing Interests Statement

The authors have declared that no competing financial, professional or personal interests exist.

Consent for publication

Both the authors contributed to the manuscript and consented to the publication of this research work.

Availability of data and material

The sources of the used data are cited in the reference list. Most of them are freely available online.

Acknowledgments

E.A. Dubowski gratefully acknowledges the support of Andrew Shaw, Hexagon, for the organising of a licence to use ERDAS Imagine and Geosystems ATCOR Atmospheric Correction Plugin for Imagine, in a personal geomorphology/geology research project entitled “Reading The Sahara: Stories in the Landscape”. The support of the team of the journal MJBAS is kindly acknowledged. We thank the reviewers for their work and helpful input.

References

[1] El-Azabi, M.H., & Sherif, F. (2011). High-resolution sequence stratigraphy of the Maastrichtian-Ypresian succession along the eastern scarp face of Kharga Oasis, southern Western Desert, Egypt. Sedimentology, 58: 579–617. https://doi.org/10.1111/j.1365-3091.2010.01175.x.

[2] Darwish, M.H., Mohamed, H.A., Elsheikh, A.E., & Tantawy, A.A. (2025). New lights on the groundwater settings of El-Kharga Oasis under over-pumping conditions, the Egyptian Western Desert. Applied Water Science, 15: 242. https://doi.org/10.1007/s13201-025-02602-2.

[3] Halipu, A., Wang, X., Iwasaki, E., Yang, W., & Kondoh, A. (2022). Quantifying water consumption through the satellite estimation of land use/land cover and groundwater storage changes in a hyper-arid region of Egypt. Remote Sensing, 14: 2608. https://doi.org/10.3390/rs14112608.

[4] Motagh, M., Walter, T.R., Sharifi, M.A., Fielding, E., Schenk, A., Anderssohn, J., & Zschau, J. (2008). Land subsidence in Iran caused by widespread water reservoir overexploitation. Geophysical Research Letters, 35: L16403. https://doi.org/10.1029/2008gl033814.

[5] Kurokami, K., Hama, A., Iwasaki, E., & Matsuoka, N. (2025). Monitoring ground surface deformation in the Kharga and Dakhla Oases in Egypt using persistent scatterer interferometry technique. Remote Sensing Applications: Society and Environment, 37: 101495. https://doi.org/10.1016/j.rsase.2025.101495.

[6] Abdelhalim, A., Abuelella, E., Sakran, S., & Said, S.M. (2023). Implementation of space-borne optical data and field investigation for geo-structural mapping of an interior rift basin: A case study from Kharit area, Southeastern Desert, Egypt. Journal of Mining and Environment, 14: 1037–1059. https://doi.org/10.22044/jme.2023.12739.2327.

[7] Alrefaee, H.A. (2017). Crustal modeling of the central part of the Northern Western Desert, Egypt using gravity data. Journal of African Earth Sciences, 129: 72–81. https://doi.org/10.1016/j.jafrearsci.2016.12.012.

[8] Rashwan, M., Sawires, R., Radwan, A.M., Sparacino, F., Peláez, J.A., & Palano, M. (2021). Crustal strain and stress fields in Egypt from geodetic and seismological data. Remote Sensing, 13: 1398. https://doi.org/10.3390/rs13071398.

[9] Sakran, S., & Said, S.M. (2018). Structural setting and kinematics of Nubian fault system, SE Western Desert, Egypt: An example of multi-reactivated intraplate strike-slip faults. Journal of Structural Geology, 107: 93–108. https://doi.org/10.1016/j.jsg.2017.12.006.

[10] US Geological Survey (USGS), Earth Explorer. Available online: https://earthexplorer.usgs.gov/. Accessed: September 2025.

[11] European Space Agency (ESA), Copernicus Browser. Available online: https://dataspace.copernicus.eu/browser/. Accessed: May–September 2025.

[12] NASA Earth Data Search. Available online: https://search.earthdata.nasa.gov/search. Accessed: May–September 2025.

[13] NASA Earth Data, Alaska Satellite Facility (ASF) Data Search. Available online: https://search.asf.alaska.edu/#/. Accessed: May–September 2025.

[14] Japan Aerospace Exploration Agency (JAXA-EORC), PALSAR-2 Global Forest/Non-forest Map "2023". Available online: https://www.eorc.jaxa.jp/alos/en/palsar_fnf/data/2023/map.htm. Accessed: May–September 2025.

[15] Mansour, K., Zaher, M.A., Deep, M.A., Medhat, N., Ebrahim, S., & Mohamed, A. (2024). Validation of ALOS/PALSAR subsurface penetration depth in Farafra Oasis as an arid region based on field ground-penetrating radar measurements. Sensing and Imaging, 25: 21. https://doi.org/10.1007/s11220-024-00472.

[16] Theilen-Willige, B. (2024). Overview of fault zones based on remote sensing data as contribution to the safety of infrastructure and land use in southern Egypt. Prevention and Treatment of Natural Disasters, 3: 17–50. https://doi.org/10.54963/ptnd.v3i1.227.

[17] Trinh, P.T., Vinh, H.Q., Van Huong, N., & Van Liem, N. (2013). Active fault segmentation and seismic hazard in Hoa-Binh reservoir, Vietnam. Central European Journal of Geosciences, 5: 223–235. https://doi.org/10.2478/s13533-012-0128-5.

[18] International Seismological Centre (ISC), Event Catalogue Search. Available online: http://www.isc.ac.uk/iscbulletin/search/bulletin/interactive/. https://doi.org/10.31905/d808b830. Accessed: May–September 2025.

[19] EMSC Euro-Mediterranean Seismological Centre, Earthquake Data. Available online: http://www.emsc-csem.org/. Accessed: May–September 2025.

[20] USGS, Search Earthquake Catalog. Available online: https://earthquake.usgs.gov/earthquakes/search/. Accessed: May–September 2025.

[21] Salman, A.B., Howari, F.M., El-Sankary, M.M., Wali, A.M., & Saleh, M.M. (2010). Environmental impact and natural hazards on Kharga Oasis monumental sites, Western Desert of Egypt. Journal of African Earth Sciences, 58: 341–353. https://doi.org/10.1016/j.jafrearsci.2010.03.011.

[22] Weather Online, Online Services, UK. Available online: https://www.weatheronline.co.uk/weather/maps/city?wmo=62435&cont=afri&land=eg&art=wdr&level=162&mod=tab. Accessed: September 2025.

[23] Arab Nubia Group Blog: GIS, Remote Sensing & General Applications. Available online: https://blog.arabnubia.com/. Accessed: September 2025.

[24] Boukhlef, D., Allali, M., Hadidi, A., & Saadi, Z. (2023). Corrosion protection of a pivot installed at URERMS, Adrar. In 1st International Conference on Material Science and Applications, Feb. 2023, Khenchela, Algeria. https://www.researchgate.net/publication/368468423.

[25] Helmi, A.M., & Zohny, O. (2020). Flash flood risk assessment in Egypt. In Negm, A.M. (Eds.), Flash Floods in Egypt. Advances in Science and Technology & Innovation, Springer Nature, Pages 295–317. https://doi.org/10.1007/978-3-030-29635-3_13.

[26] ESRI Water Balance App. Available online: https://livingatlas.arcgis.com/waterbalance/. Accessed: September 2025.

[27] NASA WorldView. Available online: https://worldview.earthdata.nasa.gov/. Accessed: September 2025.

[28] Bravard, J.P., Mostafa, A., Garcier, R., Tallet, G., Ballet, P., et al. (2016). Rise and fall of an Egyptian oasis: artesian flow, irrigation soils, and historical agricultural development in El-Deir, Kharga Depression, Western Desert of Egypt. Geoarchaeology, 31: 467–486. https://doi.org/10.1002/gea.21566.

[29] Brandes, C., Tanner, D.C., Fossen, H., Halisch, M., & Müller, K. (2022). Disaggregation bands as an indicator for slow creep activity on blind faults. Communications Earth & Environment, 3: 99. https://doi.org/10.1038/s43247-022-00423-8.

[30] Moustafa, S.S.R., Abdalzaher, M.S., & Abdelhafiez, H.E. (2022). Seismo-lineaments in Egypt: analysis and implications for active tectonic structures and earthquake magnitudes. Remote Sensing, 14: 6151. https://doi.org/10.3390/rs14236151.

[31] Abdel-Fattah, A.K., Fnais, M., Abdelwahed, M.F., El-Nekhely, A., & Farid, W. (2013). Fault orientations in the upper crust beneath an intraplate active zone in northern Egypt. Earth, Planets and Space, 65: 739–748. https://link.springer.com/content/pdf/10.5047/eps.2012.12.005.pdf.

[32] Geofabrik OpenStreetMap Data. Available online: http://download.geofabrik.de/africa.html. Accessed: September 2025.

[33] El-Rayes, A.E., Arnous, M.O., Green, D.R., & Gouda, N.F. (2023). Geo-hazards assessment of the new-found industrial communities: an example from the 10th of Ramadan Industrial Region, Egypt. Environmental Systems Research, 12: 21. https://doi.org/10.1186/s40068-023-00306-7.

[34] The Cabinet of Egypt, Information and Decision Support Center (2017). National Strategy for Disaster Risk Reduction 2030. Crisis Management and DRR Sector. https://www.preventionweb.net/files/57333_egyptian nationalstrategyfordrrengli.pdf. Accessed: September 2025.

[35] Kumari, S., Agarwal, S., Agrawal, N.K., Agarwal, A., & Garg, M.C. (2024). A comprehensive review of remote sensing technologies for improved geological disaster management. Geological Journal, 60: 223–235. https://doi.org/10.1002/gj.5072.

[36] Guikema, S. (2020). Artificial intelligence for natural hazards risk analysis: potential, challenges, and research needs. Risk Analysis, 40: 1000–1013. https://doi.org/10.1111/risa.13476.

[37] Gupta, T., & Roy, S. (2024). Applications of artificial intelligence in disaster management. In ICCAI 2024: 10th International Conference on Computing and Artificial Intelligence, Bali Island, Indonesia, April 2024. https://doi.org/10.1145/3669754.3669802.